Study on redundancy resolution algorithm of humanoid

Dongsu Yoo, Byungrok So, Jaeyeon Choi, Byungju Yi* and Wheekuk Kim**

* School of Electrical Engineering and Computer Science, HANYANG UNIVERSITY
1271, Sa 1-Dong, Sangrok-ku, Ansan, Kyunggi-do, 426-791, KOREA
** Department of Control and Instrumentation Eng,, KOREA UNIVERSITY
208, Seochang-dong, Chochiwon-up, yonki-kun, Chungnam, 339-700, KOREA

Abstract: Humans usually employ more joints than they actually need, and thus they can be categorized as a kinematically redundant system. Therefore, the behavior of the human body can be analyzed by several redundancy resolution algorithms. Different from typical industrial robots that are fixed to the ground, the COG/ZMP condition should be taken into account in the human body motion in order not to fall down. Thus a COG/ZMP stability index is employed as a measure of stability. Kinematic redundancy inherent in the human body can be exploited to satisfy the COG/ZMP condition. Simulation result shows that the COG/ZMP condition can be satisfied by exploiting the null space motion of the kinematically redundant human body model.

Keywords: COG, ZMP, Human Body Motion, Stability Index

1. INTRODUCTION

Differently from any other type of robot, humanoid-biped robots are required to have mobility enough to move various types of terrain such as plain ground, rough terrain, slope, stair and bumpy ground. And due to complexity and uncertainty in the walking motion of the biped robots, the stability of robots has been one of the major issues for research of the biped robot. Since Vukobratovic [1] proposed the concept of ZMP in 1970, ZMP has been employed as the criterion of the dynamic stability of the biped robot. To effectively adapt different walking environments and to secure the stability of the biped robot during walking motion, the biped robot had better be designed to have more degrees of freedom than required simply to follow the walking motion, by designing it as a redundant mechanism [6]. Recently, as an effort to resolve this kinematic redundancy of the biped robot, Kim, et al [2] proposed a dynamic control algorithm of a mobile robot system having kinematic redundancy by using a potential function that measures the stability degree of ZMP.

In this paper, motion-planning algorithms for humanoid are investigated with consideration of both COG and ZMP conditions. A potential function that measures the stability for COG and ZMP are employed as the performance index. The kinematic redundancy inherent to the human body is exploited to satisfy the COG/ZMP conditions. The effectiveness of the proposed algorithms is verified through simulations.

2. DEFINATION OF COG AND ZMP

2.1 Definition of COG(Center of Gravity)

COG is the point on the floor where the resultant moment occurred by the gravity is zero. COG criterion is used in static state or in very slow motion. When COG is in the support area, the robot is statically in the stable state. However, if COG is out of the support area, the robot will fall down unless appropriate external forces/torques are applied.

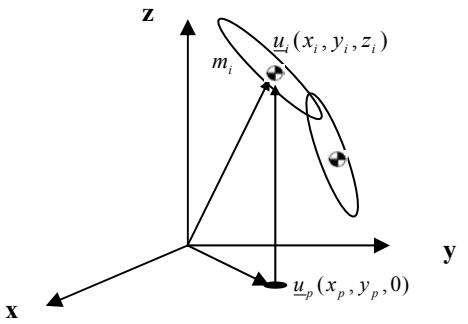

Fig 1. Calculation of COG

In Fig. 1, the mass of the i-th link is m_i and the position of the center of that link is $\underline{u}_i(x_i,y_i,z_i)$ with respect to the origin of the reference frame. Supposing that an arbitrary position $\underline{u}_p(x_p,y_p,0)$ on the floor (x-y plane) be the point where the resultant moment occurred by the acceleration of gravity is zero, we can derive the following equation

$$\sum_i m_i \underline{g} \times (\underline{u}_i - \underline{u}_p) = \underline{0}, \tag{1}$$

where

$$\underline{u}_i = \begin{bmatrix} x_i & y_i & z_i \end{bmatrix}^T, \quad \underline{u}_p = \begin{bmatrix} x_p & y_p & 0 \end{bmatrix}^T \text{ and } \underline{g} = \begin{bmatrix} 0 & 0 & g \end{bmatrix}^T$$

And (1) can be expressed as

$$\sum_i m_i g(x_p - x_i) = 0 \tag{2}$$

and

$$\sum_i m_i g(y_p - y_i) = 0. \tag{3}$$

Now, COG point existing on the x-y plane is obtained as [8]

$$x_p = x_{COG} = \frac{\sum_i m_i x_i}{\sum_i m_i} \tag{4}$$

and

$$y_p = y_{COG} = \frac{\sum_i m_i y_i}{\sum_i m_i}. \tag{5}$$

2.2 Definition of ZMP(Zero Moment Point)

ZMP is the point at which the resultant moment occurred by gravity acceleration and inertial force is zero. ZMP is initially proposed by Vukobratovic [1] and it has been employed as the criterion of stability of walking robots. ZMP must be also placed in the support area like COG, in order for the robot to be kept stable. But the robot becomes unstable and fall down when ZMP goes out of the support area.

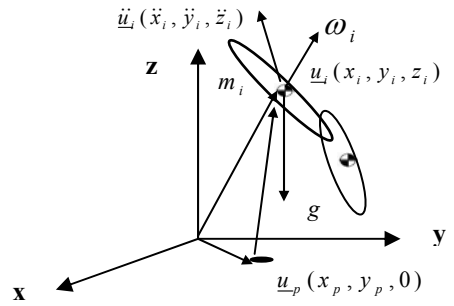

Fig. 2. Calculation of ZMP

In Fig. 2, $\underline{\ddot{u}}_i(\ddot{x}_i,\ddot{y}_i,\ddot{z}_i)$, ω_i and I_i denotes the acceleration at the center of the i-th link, the angular acceleration at the center of the i-th link, and the inertial matrix, respectively. If the point $\underline{u}_p(x_p,y_p,0)$ on the x-y plane is the position where the summation of the moment is zero, we have [4][9]

$$\sum_i(\underline{u}_i-\underline{u}_p)\times m_i(\underline{\ddot{u}}_i-g)+\sum_i(I_i\underline{\dot{\omega}}_i+\underline{\omega}_i\times I_i\underline{\omega}_i)=0. \quad (6)$$

Substituting the components of the vectors into (6) gives the position of ZMP as

$$x_{zmp}=\frac{\sum_i m_i(\ddot{z}_i+g)x_i-\sum_i m_i\ddot{x}_i z_i+(\tau_i)_y}{m_i(\ddot{z}_i+g)} \quad (7)$$

and

$$y_{Zmp}=\frac{\sum_i m_i(\ddot{z}_i+g)y_i-\sum_i m_i\ddot{y}_i z_i-(\tau_i)_x}{\sum_i m_i(\ddot{z}_i+g)}. \quad (8)$$

3. STABILITY INDEX AND REDUNDANCY RESOLUTION ALGORITHMS

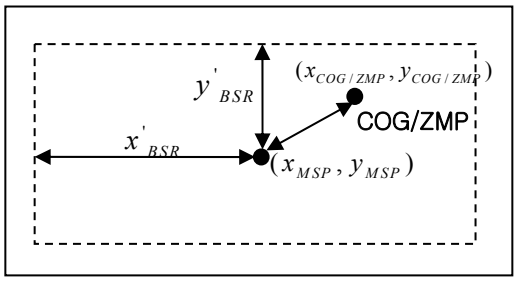

Fig. 3. Diagram of stable region

Kim, et al [2] proposed a stability index given by

$$\Phi(\underline{\theta})=\left(1-\left(\frac{x_{COG/ZMP}-x_{MSP}}{x_{BSR}}\right)^2\right)\left(1-\left(\frac{y_{COG/ZMP}-y_{MSP}}{y_{BSR}}\right)^2\right), \quad (9)$$

under the assumption boundary of stable region is a rectangular shape. $(x_{COG/ZMP},y_{COG/ZMP})$ is the position of COG or ZMP, and (x_{MSP},y_{MSP}) denotes the position of the most stable position. x_{BSR} is defined as the distance from the most stable point to the boundary stable region in the x-direction, and y_{BSR} is considered as that in the y-direction.

In this paper, separated stability indices for each direction, given by

$$\Phi_x=1-\left(\frac{x_{COG/ZMP}-x_{MSP}}{x_{BSR}}\right)^2 \quad (10)$$

and

$$\Phi_y=1-\left(\frac{y_{COG/ZMP}-y_{MSP}}{y_{BSR}}\right)^2 \quad (11)$$

will be employed. Each of these two indices represents stability margin along the x- and y-direction, respectively. Thus, two conditions given by (10) and (11) should be satisfied independently, but simultaneously.

When $\Phi<0$, COG (or ZMP) is out of the boundary of stable region. That is, the distance between COG (or ZMP) and the most stable region is longer than distance between the boundary of the stable region and the most stable point. Since the distance between COG (or ZMP) and the most stable region is shorter than the distance between the boundary of stable region and the most stable point, COG (or ZMP) is in the boundary of stable region when $0<\Phi<1$. If $\Phi=1$, the position of COG (or ZMP) is coincident with the most stable point. [2][3].

3.1 COG Stability Algorithm

If the stability index is set to be 1, it represents the most stable case. When we differentiate the stability index equation with respect to time, two equations are derived as follows:

$$\dot{\Phi}_x=B_x(\underline{\theta})\underline{\dot{\theta}}=0 \quad (12)$$

and

$$\dot{\Phi}_y=B_y(\underline{\theta})\underline{\dot{\theta}}=0, \quad (13)$$

where

$$B_x(\underline{\theta})=\left(\frac{-2(x_{COG}-x_{MSP})}{x_{BSR}}\right)\left(\frac{\partial x_{COG}}{\partial\underline{\theta}}\right) \quad (14)$$

and

$$B_y(\underline{\theta})=\left(\frac{-2(y_{COG}-y_{MSP})}{y_{BSR}}\right)\left(\frac{\partial y_{COG}}{\partial\underline{\theta}}\right). \quad (15)$$

By combining (12) and (13), we have

$$\underline{\dot{\Phi}}=B(\underline{\theta})\underline{\dot{\theta}}=\underline{0}, \quad (16)$$

where

$$B(\underline{\theta})=\left[B_x(\underline{\theta})\ \ B_y(\underline{\theta})\right]^T \text{ and } \Phi(\underline{\theta})=\left[\Phi_x(\underline{\theta})\ \ \Phi_y(\underline{\theta})\right]^T.$$

3.2 Augmented Jacobian Method for COG

The kinematic relationship between the operational vector $\underline{\dot{u}}$ and the joint velocity vector $\underline{\dot{\theta}}$ can be written as

$$\underline{\dot{u}}=J\underline{\dot{\theta}}. \quad (17)$$

Now, augmenting (16) and (17) into one matrix form yields

$$\begin{bmatrix}\underline{\dot{u}}\\0\end{bmatrix}=\begin{bmatrix}J\\B\end{bmatrix}\underline{\dot{\theta}}. \quad (18)$$

The general solution of (18) is represented as

$$\underline{\dot{\theta}}=\begin{bmatrix}J\\B\end{bmatrix}^+\begin{bmatrix}\underline{\dot{u}}\\0\end{bmatrix}+\left(I-\begin{bmatrix}J\\B\end{bmatrix}^+\begin{bmatrix}J\\B\end{bmatrix}\right)\underline{\varepsilon}, \quad (19)$$

where the superscript '+' implies a pseudo-inverse given by

$$\begin{bmatrix}J\\B\end{bmatrix}^+=\begin{bmatrix}J\\B\end{bmatrix}^T\left(\begin{bmatrix}J\\B\end{bmatrix}\begin{bmatrix}J\\B\end{bmatrix}^T\right)^{-1}.$$

If necessary, the joint angles can be obtained by numerical integration of the angular velocity vector.

3.3 Null space Method for COG

The general inverse solution of (16) can be given as

$$\underline{\dot{\theta}}=J^+\underline{\dot{u}}+([I]-J^+J)\underline{\varepsilon}, \quad (20)$$

where $\underline{\varepsilon}$ is an arbitrary vector.

When (20) is substituted into (18), we obtain

$$\underline{\dot{\Phi}}=B(\underline{\theta})(J^+\underline{\dot{u}}+([I]-J^+J)\underline{\varepsilon})=\underline{0}. \quad (21)$$

Then, from (21), $\underline{\varepsilon}$ is obtained as

$$\underline{\varepsilon}=-(B([I]-J^+J))^+BJ^+\underline{\dot{u}}. \quad (22)$$

Finally, the general inverse solution is found by inserting (22) into (20) as

$$\underline{\dot{\theta}}=J^+\underline{\dot{u}}-([I]-J^+J)(B([I]-J^+J))^+BJ^+\underline{\dot{u}}. \quad (23)$$

3.4 ZMP Stability Algorithms

Assume that the two stability indices given by

$$\Phi_x=1-\left(\frac{x_{ZMP}-x_{MSP}}{x_{BSR}}\right)^2=1 \quad (24)$$

and

$$\Phi_y = 1 - \left(\frac{y_{ZMP} - y_{MSP}}{y_{BSR}} \right)^2 = 1 \quad (25)$$

are set to be 1 for the best stability.

Then, we have

$$x_{ZMP} - x_{MSP} = 0 \quad (26)$$

and

$$y_{ZMP} - y_{MSP} = 0. \quad (27)$$

Now substituting (7) and (8) into equation (26) and (27) yields

$$\frac{\sum_i m_i(\ddot{z}_i - g)x_i - \sum_i m_i \ddot{x}_i z_i + \sum_i (\tau_y)_i}{\sum_i m_i(\ddot{z}_i - g)} - x_{MSP} = 0 \quad (28)$$

and

$$\frac{\sum_i m_i(\ddot{z}_i - g)y_i - \sum_i m_i \ddot{y}_i z_i - \sum_i (\tau_x)_i}{\sum_i m_i(\ddot{z}_i - g)} - y_{MSP} = 0. \quad (29)$$

Rearranging (28) and (29) gives

$$\sum_i m_i \ddot{z}_i x_i - \sum_i m_i \ddot{x}_i z_i - \sum_i m_i \ddot{z}_i x_{MSP} - \sum_i \tau_y = C_x \quad (30)$$

and

$$\sum_i m_i \ddot{z}_i y - \sum_i m_i \ddot{y}_i z_i - \sum_i m_i \ddot{z}_i y_{MSP} - \sum_i \tau_x = C_y, \quad (31)$$

where

$$C_x = \sum_i m_i (x_i - x_{MSP}) g$$

and

$$C_y = \sum_i m_i (y_i - y_{MSP}) g.$$

The inertial moment occurring at the center of the i-th link is expressed as [10]

$$\underline{\tau}_i = [I_i]\ddot{\underline{\theta}} + \underline{\dot{\omega}} \times [I_i]\underline{\dot{\theta}} = [I_i]\ddot{\underline{\theta}} + \dot{\underline{\theta}}^T [P^{jk}]\underline{\dot{\theta}}. \quad (32)$$

In the meanwhile, the acceleration of the operational point given by

$$\ddot{\underline{u}} = [J]\ddot{\theta} + \dot{\underline{\theta}}^T [H]\underline{\dot{\theta}} \quad (33)$$

can be decomposed as three components

$$\ddot{\underline{x}}_i = [J_i]_{1;}\ddot{\underline{\theta}} + \dot{\underline{\theta}}^T [H_i]_{1;;}\underline{\dot{\theta}},$$

$$\ddot{\underline{y}}_i = [J_i]_{2;}\ddot{\underline{\theta}} + \dot{\underline{\theta}}^T [H_i]_{2;;}\underline{\dot{\theta}},$$

$$\ddot{\underline{z}}_i = [J_i]_{3;}\ddot{\underline{\theta}} + \dot{\underline{\theta}}^T [H_i]_{3;;}\underline{\dot{\theta}}.$$

Substituting these components into (30) and (31) and reformulation (30), (31), and (32) in a matrix form yields

$$\underline{C} = [J_m]\ddot{\underline{\theta}} + \dot{\underline{\theta}}^T [H_m]\underline{\dot{\theta}}, \quad (34)$$

where

$$[J_m] = \sum_i \begin{bmatrix} m_i x_i [J_i]_{3;} - m_i z_i [J_i]_{1;} - m_i y_{MSP} [J_i]_{3;} \\ m_i y_i [J_i]_{3;} - m_i z_i [J_i]_{2;} - m_i y_{MSP} [J_i]_{3;} \\ [I_i] \end{bmatrix}$$

and

$$[H_m] = \sum_i \begin{bmatrix} m_i x_i [H_i]_{3;;} - m_i z_i [H_i]_{1;;} - m_i x_{MSP} [H_i]_{3;;} \\ m_i y_i [H_i]_{3;;} - m_i z_i [H_i]_{2;;} - m_i y_{MSP} [H_i]_{3;;} \\ [P_i^{jk}] \end{bmatrix}.$$

3.5 Augmented Jacobian Method for ZMP

(33) and (34) can be augmented as one matrix form given by

$$\begin{bmatrix} \ddot{\underline{u}} \\ \underline{C} \end{bmatrix} = \begin{bmatrix} J_m \\ J \end{bmatrix} \ddot{\underline{\theta}} + \dot{\underline{\theta}}^T \begin{bmatrix} H_m \\ H \end{bmatrix} \dot{\underline{\theta}}. \quad (35)$$

Then, the angular acceleration vector is obtained as

$$\ddot{\underline{\theta}} = \begin{bmatrix} J_m \\ J \end{bmatrix}^+ \left(\begin{bmatrix} \ddot{\underline{u}} \\ C \end{bmatrix} - \dot{\underline{\theta}}^T \begin{bmatrix} H_m \\ H \end{bmatrix} \dot{\underline{\theta}} \right) + \left([I] - \begin{bmatrix} J_m \\ J \end{bmatrix}^+ \begin{bmatrix} J_m \\ J \end{bmatrix} \right) \underline{\varepsilon} \quad (36)$$

by taking the pseudo-inverse of (35), where $\underline{\varepsilon}$ is an arbitrary vector.

3.6 . Null space Method for ZMP

As an alternative method, we can employ the null space solution to improve the COG or ZMP stability. The general inverse solution of (33) is given by

$$\ddot{\underline{\theta}} = J^+ \left(\ddot{\underline{u}} - \dot{\underline{\theta}}^T [H]\underline{\dot{\theta}} \right) + ([I] - J^+ J)\underline{\varepsilon}. \quad (37)$$

If we substitute (37) into (34), we can solve for $\underline{\varepsilon}$ as below

$$\underline{\varepsilon} = [J_m(I - J^+ J)]^+ \left(-J_m J^+ \left(\ddot{\underline{u}} - \dot{\underline{\theta}}^T [H]\dot{\underline{\theta}} \right) - \underline{C} - \dot{\underline{\theta}}^T [H_m]\dot{\underline{\theta}} \right). \quad (38)$$

We can solve the angular acceleration vectors by substituting (38) into (37). Integrating the acceleration vectors twice with respect to time yields the joint angles.

4. SIMULATIONS

Because the number of the input joint angles is more than the number of the output coordinates, the system given in Fig. 4 can be called a kinematically redundant system. The system is to control y and z positions with three active inputs for this operation. Thus, one kinematic redundancy exists, which can be exploited to improve the ZMP stability.

4.1 Simulation Parameters

Simulation is performed to show the efficiency of COG and ZMP algorithms [8].

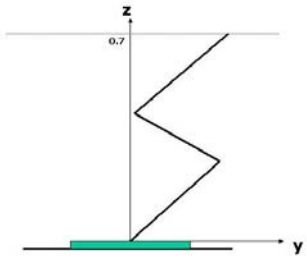

Fig. 4. Simulation model

Table 1: Link Parameters and Simulation Condition

	Link 1	Link 2	Link 3
Initial angle	59.87°	141.87°	-133.84°
Length	0.4428m	0.4410m	0.5184m
Mass	6.02kg	14.00kg	35.00kg
Velocity profile		$v(t) = -0.1\sin(t)\, m/s$	
y_{MSP}		$(0,0)$	
y_{BSR}		$\pm 0.1m$	

The lengths, masses, and initial angles of the links of the given model are listed in Table 1. The support length is given 0.1m in both positive and negative y-directions. And the end effecter moves from left to right for 3 seconds with the sinusoidal velocity profile given in the table, while keeping z-position fixed(z=7).

4.2 Simulation for COG Algorithm

When we consider a planar model, Φ_x of COG stability indices is disappeared. So, COG stability index can be written as

$$\Phi_y(\underline{\theta}) = 1 - \left(\frac{y_{COG} - y_{MSP}}{y_{BSR}} \right)^2 = 1. \quad (39)$$

Differentiating (39) with respect to the time, we have

$$\dot{\Phi}_y(\underline{\theta}) = B(\underline{\theta})\dot{\underline{\theta}} = 0, \quad (40)$$

where

$$B(\underline{\theta}) = \left(\frac{-2(y_{COG} - y_{MSP})}{y_{BSR}^2} \right) \left(\frac{\partial y_{COG}}{\partial \theta_1} \quad \frac{\partial y_{COG}}{\partial \theta_2} \quad \frac{\partial y_{COG}}{\partial \theta_3} \right)$$

and

$$\dot{\underline{\theta}} = \left(\dot{\theta}_1 \quad \dot{\theta}_2 \quad \dot{\theta}_3 \right)^T.$$

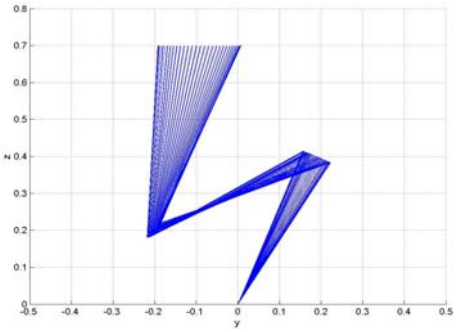

(a) Motion using the particular solution

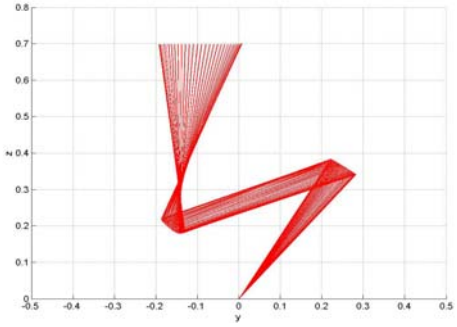

(b) Motion using COG algorithm

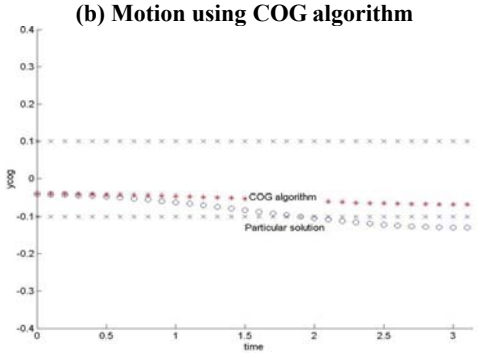

(c) COG trajectory

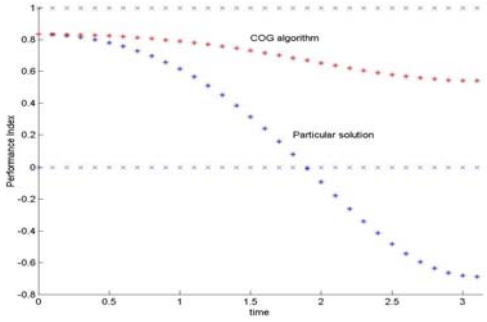

(d) Potential function trajectory

Fig. 5. Simulation result

Fig 5(a) illustrates the behavior of the manipulator in the case of not applying COG algorithm, using only the particular solution given by (20). Fig. 5(b) shows the movement of the manipulator when COG algorithm is applied by using the null-space solution. Fig. 5(c) shows that COG algorithm ensures the COG stability since the trajectory is inside the footprint. Also, Fig. 5(d) shows that the stability index is between 0 and 1, implying that COG algorithm is effective.

4.3 Limitation of COG Algorithm

When the velocity of manipulator is very slow, COG trajectory is almost coincident with ZMP. However, when the velocity increases, the moment caused by the acceleration applying to the z-direction increases gradually. Thus, the stability condition can't be satisfied just by relying on COG.

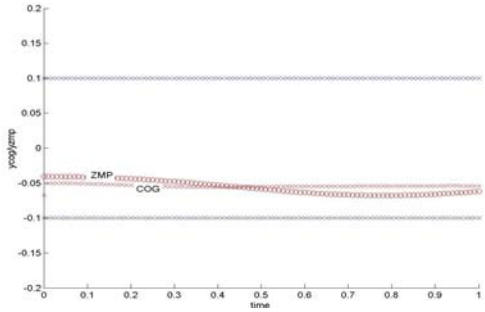

(a) $\dot{y} = 0.4\sin(4t)$

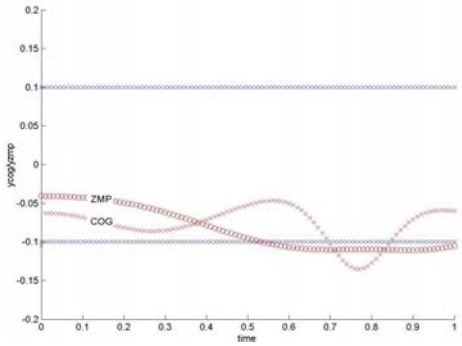

(b) $\dot{y} = 1.0\sin(4t)$

Fig. 6. COG and ZMP trajectories

For example, Fig. 6(a) and Fig. 6(b) shows the COG and ZMP trajectories when the amplitude of sine wave is 0.4 and 1.0, respectively. When it is 0.4, the gap between COG and ZMP trajectory is small, but when it is 1.0, the shape of COG trajectory is significantly different from that of ZMP. Thus, as the velocity of manipulator becomes fairly fast, ZMP algorithm is more accurate and practical than COG algorithm.

4.4 Simulation for ZMP Algorithm

The simulation is performed for the same condition as Fig. 4, except the mass of the third link reduced from 35kg to 12kg. And only the y-element of the ZMP condition is considered. The ZMP stability index that is equivalent to (31) is employed

$$\Phi_y(\underline{\theta}) = 1 - \left(\frac{y_{ZMP} - y_{MSP}}{y_{BSR}} \right)^2 = 1. \quad (41)$$

Since the given system is operated in a planar domain, the inertial moment term is simplified as

$$\underline{\tau}_i = [I_i]\ddot{\underline{\theta}} = [I_1^{xx} + I_2^{xx} + I_3^{xx} \quad I_2^{xx} + I_3^{xx} \quad I_3^{xx}]\ddot{\underline{\theta}}. \quad (42)$$

Noting that the system has only one redundancy, the solution similar to (35) is obtained as

$$\ddot{\underline{\theta}} = \begin{bmatrix} J_m \\ J \end{bmatrix}^{-1} \left(\begin{bmatrix} \ddot{\underline{u}} \\ C \end{bmatrix} - \dot{\underline{\theta}}^T \begin{bmatrix} H_m \\ H \end{bmatrix} \dot{\underline{\theta}} \right), \tag{43}$$

where

$$\underline{u} = [y \quad z]^T, \quad \underline{\theta} = [\theta_1 \quad \theta_2 \quad \theta_3]^T,$$

$$[J_m] = \begin{bmatrix} \sum_{i=1}^{3} (m_i y_i [J_i]_{2;} - m_i z_i [J_i]_{1;} - m_i y_{ZMP} [J_i]_{2;}) \\ [I_1^{xx} + I_2^{xx} + I_3^{xx} \quad I_2^{xx} + I_3^{xx} \quad I_3^{xx}] \end{bmatrix}$$

and

$$[H_m] = \begin{bmatrix} \sum_{i=1}^{3} (m_i y_i [H_i]_{3;;} - m_i z_i [H_i]_{2;;} - m_i y_{MSP} [H_i]_{3;;} \\ [0] \end{bmatrix}.$$

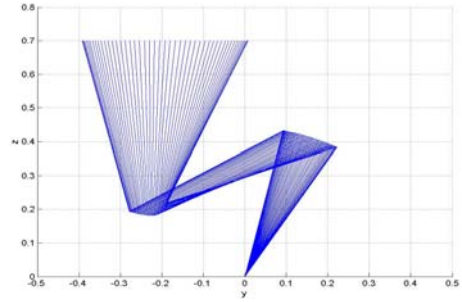

(a) The result of not applying ZMP algorithm

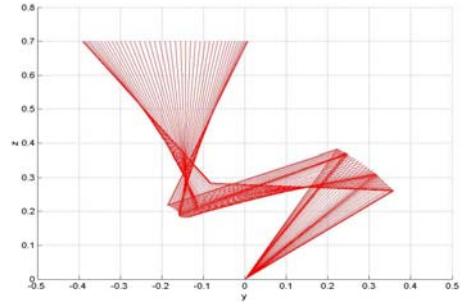

(b) The result of applying ZMP algorithm

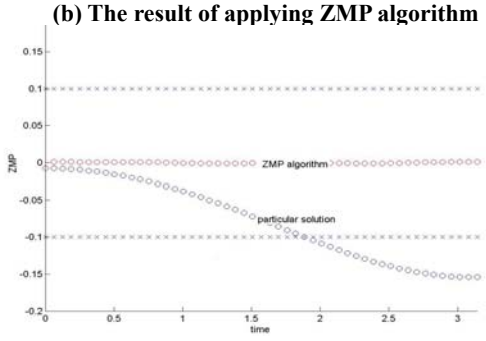

(c) ZMP trajectory

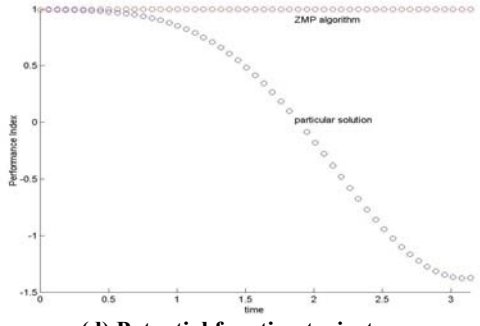

(d) Potential function trajectory

Fig. 7. Simulation results

In this simulation, we use $\dot{y} = 0.2\sin(t)$ as the velocity profile of the end position. Fig. 7(a) shows the case of not applying ZMP algorithm. Fig. 7(b) is the case of using ZMP algorithm. As shown in the figures, the upper ZMP trajectory follows the value, '0', implying that the kinematic redundancy was properly exploited to improve the ZMP stability. However, we can observe the phenomenon that the manipulator movement becomes unstable at the last part of the trajectory. This is due to abrupt increase of joint acceleration due to wound up of null space dynamics.

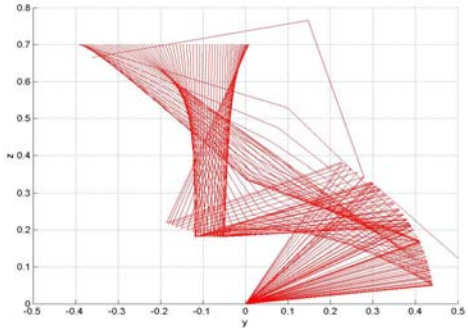

(a) The behavior of manipulator when the mass of the third link is 35kg

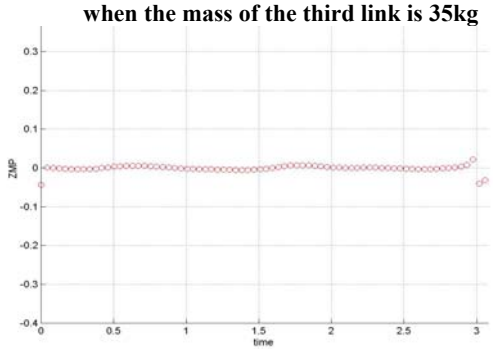

(b) ZMP Trajectory

Fig. 8. The movement of manipulator and its ZMP trajectory when mass of third link is 35kg

To cope with this unstable movement, a null space damping [5] will be employed. That is, an additional $\underline{\varepsilon}$ given by

$$\underline{\varepsilon}' = -\begin{bmatrix} w & 0 & 0 \\ 0 & w & 0 \\ 0 & 0 & w \end{bmatrix} \dot{\underline{\theta}} \tag{44}$$

will be incorporated into (38), which tends to damp out the acceleration wound up by the uncontrollable null space dynamics [5]. When we substitute the additional $\underline{\varepsilon}$ vector into (36), the ZMP trajectory becomes more stable as shown in Fig. 9.

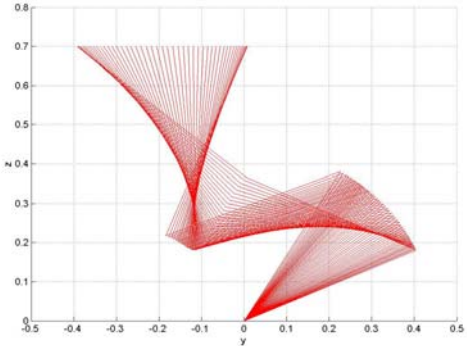

(a) When applying damping equation (w=16)

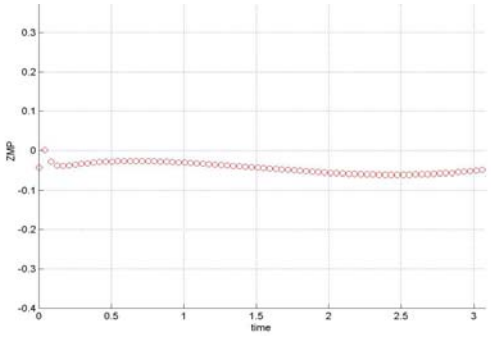

(b) ZMP trajectory

Fig. 9. The movement of manipulator and its ZMP trajectory when null space damping is given.

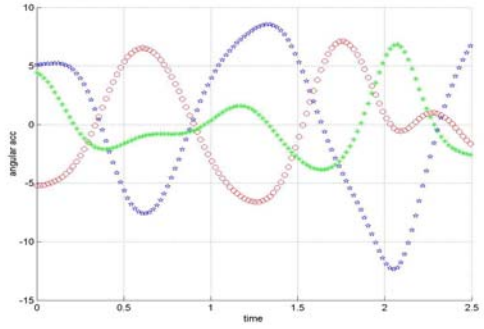

(a) The angular acceleration of joints without null space damping

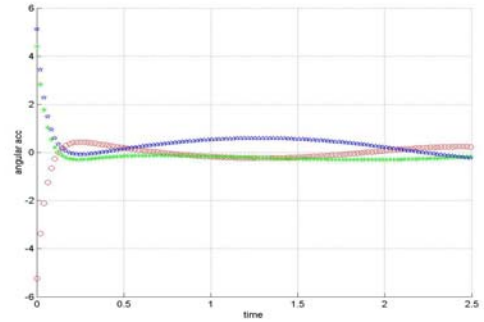

(b) The angular acceleration of joints with null space damping

Fig. 10. The angular acceleration with and without null space damping

Fig. 10 also shows the variation of the joint accelerations of the two cases. When the third mass becomes heavier, the angular acceleration of each links is increased and the motion of the links becomes unstable. The damping matrix plays an important role in reducing the acceleration of links and then decreasing the instability of link movement.

5. CONCLUSION

In this paper, we employed the stability indices associated with COG and ZMP. Those stability indices are transformed to an expanded kinematic equation, which is augmented to exploit the null space due to kinematic redundancy. Simulations illustrated the effect of COG and ZMP algorithms in a kinematically redundant system. It was shown that the COG and ZMP condition could be improved by employing the null space motion. As future works, we need to apply these algorithms to more general spatial models, and to study efficient way of using null space damping

REFERENCES

[1] Vukobratovic, M., A.A. Frank, and D. Jricic. "On the stability of biped locomotion," *IEEE Trans. On Biomedical Engineering,* BME17-1, pp. 25-36, 1970.

[2] J. Kim, W. Chung, Y. Youm, and B. Lee, "Real-time ZMP compensation method using null motion for mobile manipulators," *IEEE International Conference on Robotics & Automation*, pp. 1967-1972, 2002.

[3] Q. Huang, S. Sugano, and I. Kato, "Stability control for a mobile manipulator using a potential method," *Proc., IEEE/RSJ Int. Conf. On Intelligent Robots and Systems*, pp. 832-838, 1993.

[4] A. Dasgupta and Y. Nakamura, "Walking feasible walking motion of humanoid robotics from human motion capture data," *IEEE International Conference on Robotics and Automation*, pp. 1044-1049, 1999.

[5] H. Kang and R. A. Freeman, "Joint torque optimization of redundant manipulators via the null space damping method," *IEEE International Conference on Robotics and Automation*, pp. 520-525, 1992.

[6] F. Amironche, C. Tung, G. Andersson, and R. Natarajan, "Redundancy modeling of optimum lifting conditions," *Advances in Bioengineering ASME*, BED-Vol. 20, pp. 509-512, 1991.

[7] D. Chaffin and G. Andersson, "Occupational biomechanics," pp. 62-69, 1984.

[8] J. Lee, K. Lee, I. Park, and J. Oh, "Walking and control of autonomous biped robot", *IFAC Workshop on Mobile Robot Technology*, pp.179-183, 2001.

[9] J. Park, "Analysis and control of kinematically redundant manipulators: An approach based on kinematically decoupled joint space decomposition". PhD thesis, POSTECH, Korea, 2000.

[10] A. Bedford and W. Fowler, "Engineering mechanics: dynamics," 2nd Edition, *Addison Wesley Longman, Inc.*, pp. 490-492, 1999.